Two- and three-mode dressed entanglement multichannel in cavity four-wave mixing of Pr^{3+}: YSO

2016 Laser Phys. Lett. 13 115701

(http://iopscience.iop.org/1612-202X/13/11/115701)

IOP Publishing | Astro Ltd
Laser Physics Letters
Laser Phys. Lett. **13** (2016) 115701 (13pp)
doi:10.1088/1612-2011/13/11/115701

Letter

Two- and three-mode dressed entanglement multichannel in cavity four-wave mixing of Pr^{3+}:YSO

Xiaoli Wang[1], Zepei Li[1,3], Feng Wen[1], Yun Xu[1], Lingxiang Peng[3], Wei Niu[3], Peiyu Li[3] and Yanpeng Zhang[2]

[1] School of Science, Xi'an Jiaotong University, Xi'an 710049, People's Republic of China
[2] Key Laboratory for Physical Electronics and Devices of the Ministry of Education and Shaanxi Key Lab of Information Photonic Technique, Xi'an Jiaotong University, Xi'an 710049, People's Republic of China
[3] Xi'an Satellite Control Center, Xi'an 710043, People's Republic of China

E-mail: xlwang@mail.xjtu.edu.cn and ypzhang@mail.xjtu.edu.cn

Received 18 May 2016, revised 6 September 2016
Accepted for publication 12 September 2016
Published 20 October 2016

Abstract

We report a theoretical study into the two- and three-mode entanglement inside an atom-like optical cavity. A five-level system is considered and the influence of the multi-dressed parametric amplification four-wave mixing (PA-FWM) process on the quantum correlation of fluctuation spectra is researched. Three-mode entanglement is determined by the coupling of two nonlinear gains; one of enhanced gains via the dressing state plays a dominant role in controlling and optimizing the profile of three-mode entanglement via vacuum Rabi splitting, enhancement/suppression of entanglement as well as two-mode. Specifically, increasing the quantity of dressing fields may result in the single-channel entanglement turning into nonlocal multichannel (multiple anti-crossing behaviors). Moreover, these entanglement channels can be squashed via the lateral squeezing effect of the cavity. Such multichannel entanglement has potential applications in nonlocal quantum imaging and quantum key distribution.

Keywords: parametric processes, quantum fluctuations, optical parametric amplifiers, cascade four-wave mixing

(Some figures may appear in colour only in the online journal)

1. Introduction

Generating multi-mode entanglement with controllable quantum states is important to realize entanglement-based quantum information processing, such as quantum routing [1], quantum key distribution (QKD) [2, 3] and long-distance quantum communication [4]. Recently, the interest in utilizing continuous variables (CV) of optical fields to generate squeezing and entanglement states is increasing due to its applicability in quantum information, where field fluctuations in one of the quadratures are reduced below the shot noise. This can be used in overcoming the shot-noise precision restrictions in optical measurements [5] and realization of sub-shot-noise quantum imaging [6]. Generally speaking, techniques for producing the entanglement states are based on either parametric down-conversion [7, 8] in solid-state crystal or spontaneous parametric four-wave mixing (SP-FWM) in atomic vapors. Nowadays, the EPR (Einstein–Podolsky–Rosen) entangled state of light with quantum correlations of 8.4 dB for both amplitude and phase quadratures are experimentally produced [9] using a single non-degenerate optical parametric amplifier. However, bi-photons generated from spontaneous parametric down-conversion (SPDC) in nonlinear crystals have very wide bandwidth (>THz) and ultra-short coherence time (<ps)

[10]. In contrast, the SP-FWM process in atomic ensemble demonstrates a performance that is narrow-band (<MHz) and bi-photons with a long coherence time (>0.1–1.0 μs) [11]. Such a long coherence time allows us to access and manipulate the spatial entanglement directly. However, achieving a higher degree of entanglement via FWM in atomic vapors is limited by spontaneous emission noise. As a result of atomic coherence, electromagnetically induced transparency (EIT) [12] and dressed multi-wave mixing [13, 14] attract a lot of attention. Researches have demonstrated that the spontaneous emission noise can be reduced or eliminated by EIT [12]. In the EIT window the transmission and the absorption spectrum agrees well with calculations based, experimentally, on the double-dressing density-matrix equations[15]. Currently, in hot rubidium vapor a large number of modes of quantum-correlated beams [16] have been generated by using multiple FWM processes.

In previous studies, two beams of light could be quantum mechanically entangled through correlations of their phase and intensity fluctuations [11]. Three strong quantum correlation bright beams have been produced via two cascade FWM (TC-FWM) in experiment [16]. The influence of dark states on two-mode optical entanglement in rubidium atomic ensemble [17] and the transitions between the bright and dark states by nested and parallel double-dressing FWM have been reported [18]. The essential characteristic of such enhanced nonlinear optical processes is the controllable nonlinear susceptibility due to atomic coherence. It can be used to generate the strongly correlated three-mode bright beams [19] in a cavity with high efficiency and narrow bandwidth. Meanwhile, spatial-mode multiplexing for entanglement distribution and the suitability of FWM in atomic vapors as a resource for QKD schemes have been demonstrated [20]. At present, multiparticle entanglement has been reported comprehensively, and there are some experiments that have realized one-to-one entanglement distribution [21, 22], but up to now the investigation on quantum multichannel entanglement that realizes secure key one-to-multiple distribution in a Pr^{3+}: YSO crystal has not been reported theoretically or experimentally.

In this letter, we extend multi-dressed two-mode entanglement to the three-mode case and explore tripartite CV entanglement in an atomic-cavity coupled system. Here, we focus on the role of the multi-dressed state and nonlinear gain on the three-mode entanglement process. Based on the standard criteria proposed by van Loock *et al* [23] and enhanced nonlinear optical processes, we propose a scheme for achieving CV two- and three-mode entanglement. First, we investigated three-channel entanglement of two-mode sequential double dressing. Second, we investigated multichannel three-mode entanglement coming from TC-FWM processes with sequential and parallel double dressing and triple dressing, respectively. The entanglement maximum peak is determined by nonlinear gain and the entanglement profile is modified by the dressing field. Further, our system can be used directly in multichannel nonlocal quantum imaging. The quality of imaging, including the contrast and resolution, is significantly improved compared with the two-mode entanglement state [24] and can be well controlled by multiple parameters. The proposed method is also used in the implementation of a three-mode entangled source to achieve multichannel communication, for example, realizing secure key one-to-multiple distribution in QKD. This paper is organized as follows. In section 2, we describe the basic physics for the parametric amplification four-wave mixing (PA-FWM) and TC-FWM processes. Then, we calculate the variance for the entanglement criterion of two- and three-mode entanglement. In section 3, we present the entanglement properties with the multiple dressed fields. In section 4, we conclude the paper.

2. Basic theory

2.1. TC-FWM in atom-like cavity

A theoretical scheme for the preparation of three-mode entanglement is carried out in a sample of 0.05% rare-earth Pr^{3+} doped Y_2SiO_5 (Pr^{3+}: YSO) crystal, which has good performance and the atomic coherence are important materials for the research and development on some nonlinear optics, quantum computing and optical information storage topics. Figure 1(a) illustrates the simplified energy-level diagram of Pr^{3+}: YSO. We can analyze of the triplet energy level $^3H_4$ and doublet energy level $^1D_2$ since it is easy to identify them reliably by investigating the optical spectrum of the Pr^{3+} ions. The degeneracy of the energy levels of the Pr^{3+} is removed completely by the crystal field of YSO, where the terms in $^3H_4$ and $^1D_2$ states are split into nine and five Stark components, respectively. The Pr^{3+} impurity ions can occupy two nonequivalent cation sites (i.e. sites I and II, respectively) in the YSO crystal lattice. The energy levels of site I are labeled by a Greek letter without asterisk and the ones for site II with an asterisk as shown in figure 1(a). Actually, with induced dipole–dipole interaction, the coupling between Pr^{3+} ions localized at different cation vacancies in the YSO crystal can occur, so one can treat the two ions (at different sites) as a hetero nuclear-like molecule [25]. Therefore, we can construct a five-level diagram for the Pr^{3+} ions in Pr^{3+}: YSO crystal by coupling the corresponding laser beams as indicated in figure 1(b). The Stark level δ_0, δ_1 and δ_2 of the ground state $^3H_4$ and the lowest Stark level γ_0 and γ_0^* of excited-state $^1D_2$ are selected to couple with each other. Three corresponding laser beams are $\boldsymbol{E}_1$ (frequency ω_1, wave vector $\boldsymbol{k}_1$, Rabi frequency G_1) driving $|0\rangle(\delta_0) \leftrightarrow |1\rangle(\gamma_0^*)$ transition, $\boldsymbol{E}_2$ (ω_2, $\boldsymbol{k}_2$, G_2) driving $|0\rangle(\delta_0) \leftrightarrow |2\rangle\gamma_0$ and $\boldsymbol{E}_3$ (ω_3, $\boldsymbol{k}_3$, G_3) driving $|3\rangle(\delta_1) \leftrightarrow |2\rangle\gamma_0$. Next, we introduce the three-mode entanglement via TC-FWM in figure 1(b). Such cascade processes consist of two cascades involving closed-loop SP-FWM in a Λ-type ($|0\rangle(\delta_0) \leftrightarrow |2\rangle(\gamma_0) \leftrightarrow |3\rangle(\gamma_1)$) and a V-type ($|0\rangle(\delta_0) \leftrightarrow |1\rangle(\gamma_0) \leftrightarrow |2\rangle(\gamma_1)$) three-level sub-system. Two sub-systems can generate two kinds of non-degenerate SP-FWM processes by coupling the corresponding laser fields. When there are pumping beams $\boldsymbol{k}_2$ and $\boldsymbol{k}_3$ (propagating in the opposite directions), the Λ-type three-level subsystem generates two SP-FWM signals $\boldsymbol{E}_{S2}$ (ω_{S2}, $\boldsymbol{k}_{S2}$, G_{S2}) and $\boldsymbol{E}_{S3}$ (ω_{S3}, $\boldsymbol{k}_{S3}$, G_{S3}). Two entangled signals $\boldsymbol{k}_{S2}$ and $\boldsymbol{k}_{S3}$ are generated along different directions and satisfy phase-matching conditions $\boldsymbol{k}_{S2} = \boldsymbol{k}_2 - \boldsymbol{k}_{S3} + \boldsymbol{k}_3$ and $\boldsymbol{k}_{S3} = \boldsymbol{k}_3 - \boldsymbol{k}_{S2} + \boldsymbol{k}_2$, respectively.

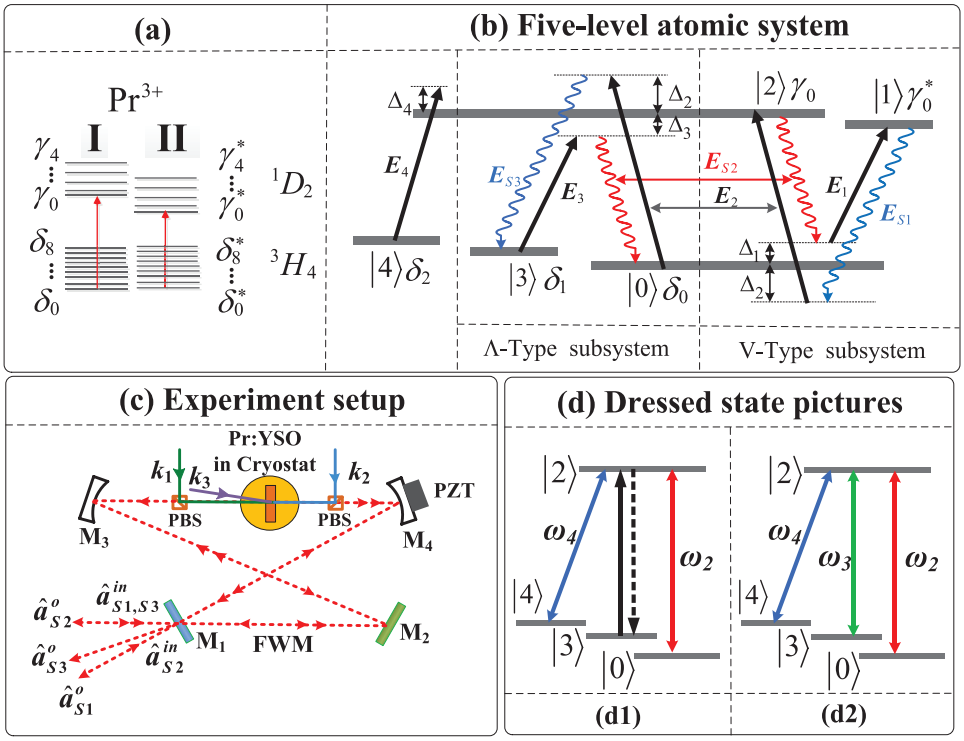

Figure 1. (a) Simplified energy-level diagram of Pr^{3+} ions in an YSO crystal. (b) Schematics diagram of five-level atom-like system in Pr^{3+}: YSO crystal for triple-photon generation by TC-FWM, made up of a Λ-type and a V-type three-level subsystem. Δ_i: frequency detuning of $\boldsymbol{E}_i$ ($i = 1$–4). δ: ground-state energy levels, γ: excited-state energy levels. ($\lambda[|0\rangle(\delta_0) \leftrightarrow |2\rangle(\gamma_0)] = 607.94$ nm, $\lambda[|0\rangle(\delta_0) \leftrightarrow |1\rangle(\gamma_0^*)] = 605.99$ nm, $\lambda[|3\rangle(\delta_1) \leftrightarrow |2\rangle(\gamma_0)] = 609.2$ nm, $\lambda[|4\rangle(\delta_2) \leftrightarrow |2\rangle(\gamma_0)] = 611.4$ nm). (c) Experimental setup of three-mode entanglement via PA-FWM. PBS: polarizing beam splitter, PZT: piezoelectric transducer. (d) Double and triple dressed state diagrams, respectively.

The conservation of energy is $\omega_{S2} + \omega_{S3} = \omega_2 + \omega_3$. The generating frequency is $\omega_i = \varpi_i + \delta$ ($i = S2$ and $S3$); here ϖ_i is center frequency and δ is the small fluctuation around ω_i. Since the SP-FWM process absorbs two photons ($\boldsymbol{E}_2$ and $\boldsymbol{E}_3$) and produces one Stokes ($\boldsymbol{E}_{S2}$) and one anti-Stokes ($\boldsymbol{E}_{S3}$) photon simultaneously, the two output photons of the SP-FWM process are highly correlated. Similarly, in the V-type sub-system the SP-FWM signals $\boldsymbol{E}_{S1}$ (ω_{S1}, $\boldsymbol{k}_{S1}$, G_{S1}) and $\boldsymbol{E}_{S2}$ are obtained from the incident beams $\boldsymbol{E}_1$ and $\boldsymbol{E}_2$. $\boldsymbol{k}_{S1}$ and $\boldsymbol{k}_{S2}$ satisfy phase-matching conditions $\boldsymbol{k}_{S2} = \boldsymbol{k}_1 - \boldsymbol{k}_{S1} + \boldsymbol{k}_2$ and $\boldsymbol{k}_{S1} = \boldsymbol{k}_1 - \boldsymbol{k}_{S2} + \boldsymbol{k}_2$, and energy conservation $\omega_{S1} + \omega_{S2} = \omega_1 + \omega_2$. Here, the fluctuations of the entangled signals $\boldsymbol{E}_{S1}$, $\boldsymbol{E}_{S2}$, and $\boldsymbol{E}_{S3}$ have zero on average and quantum-correlate with each other. The connection between these two involved closed-loop SP-FWM processes (Λ-type and V-type in figure 1(b)) mentioned above is that the cascade processes share the same pumping beam $\boldsymbol{E}_2$ and output beam $\boldsymbol{E}_{S2}$ both in frequency domain and spatial domain. TC-FWM is similar to the SP six-wave mixing (SWM) with the phase conditions $\boldsymbol{k}_{S1} + \boldsymbol{k}_{S2} + \boldsymbol{k}_{S3} = \boldsymbol{k}_1 + \boldsymbol{k}_2 + \boldsymbol{k}_3$.

Secondly, we present experimental setup of three-mode entanglement via TC-FWM in figure 1(c). Here, schematics of three-mode entanglement with incident beams $\boldsymbol{E}_1$, $\boldsymbol{E}_3$ and $\boldsymbol{E}_2$ pass through the Pr^{3+}: YSO atomic vapor in the opposite directions. Three entangled signals $\boldsymbol{k}_{S1}$, $\boldsymbol{k}_{S3}$ and $\boldsymbol{k}_{S2}$ will form three output cavity modes ($\hat{a}^{o}_{S1}$, $\hat{a}^{o}_{S3}$ and $\hat{a}^{o}_{S2}$ in figure 1(c)) and are detected by three avalanche photodiode detector devices. At the same time, to ensure high conversion efficiency of SP-FWM and suppressed collinear resonance fluorescence, we should notice that there is a small angle between $\boldsymbol{k}_1$ and $\boldsymbol{k}_3$ to separate $\hat{a}^{o}_{S3}$ and $\hat{a}^{o}_{S1}$ as shown in figure 1(c). If there is no seeding to each SP-FWM, the output states will term as three-mode squeezed vacuum states. When TC-FWM is injected with seeding beams $\hat{a}^{in}_{S1}$, $\hat{a}^{in}_{S2}$ and $\hat{a}^{in}_{S3}$ ($\boldsymbol{k}_{S1}$, $\boldsymbol{k}_{S2}$ and $\boldsymbol{k}_{S3}$ channels, correspondingly), the quantum gain can be enhanced, and the output states are three-mode squeezing quantum amplified states and the process becomes PA-FWM. In particular, when the incident beam $\boldsymbol{k}_1$ is blocked in figure 1(c), we can achieve the two-mode entangled $\hat{a}^{o}_{S2}$ and $\hat{a}^{o}_{S3}$ via PA-FWM in the Λ-type subsystem. Here, the ring cavity is formed by four mirrors with a longitudinal cavity length of 17 cm. The mirrors M_3 and M_1 are input and output mirrors with the reflectance r_3 (r_1) and transmittance t_3 (t_1) satisfying the condition $r_i^2 + t_i^2 = 1$ ($i = 1, 3$), while M_2 and M_4 are highly reflective mirrors in figure 1(c). Cavity-mode scanning and locking can be implemented by a PZT behind M_4. Since we do not consider Doppler effects, our analysis is also suitable for standing-wave cavities. For the limit of the cavity, the conical emission disappears. However, if three photons are prepared simultaneously, the entanglement amongst them still exists. Thirdly, considering the three incident beams' intensity condition $\boldsymbol{E}_2 > \boldsymbol{E}_3$ and $\boldsymbol{E}_3 \gg \boldsymbol{E}_1$, then $\boldsymbol{E}_{S1}$, $\boldsymbol{E}_{S2}$ and $\boldsymbol{E}_{S3}$ becomes dressed PA-FWM. To simplify calculation, we consider ω_{S1}, ω_{S2} and ω_{S3} as single-frequency light (i.e. $\delta = 0$), the corresponding multi-dressed

state diagrams are shown in figure 1(d). Based on the dressed state analysis, two-photon resonance results in the dark state, and the resonances of coupling field with the dressed state leading to the bright state. Through scanning different cavity detuning Δ and field detuning Δ_1 (Δ_2, Δ_3), spectrum variances of entanglement will present bright-state and dark-state controllable conversion.

Generally, the fluctuations of entangled photons $\boldsymbol{E}_{S1}$, $\boldsymbol{E}_{S2}$, and $\boldsymbol{E}_{S3}$ are quantum-correlated, and they can be used to prepare CV three-mode quadrature amplitude or phase-squeezed state of the optical field. In addition, it has been shown how to produce genuinely entangled multi-mode states by van Loock [23], and we can conclude that the sufficient inseparability criterion for any CV two- and three-mode entangled states: $\langle\delta^2(X_1-X_2)\rangle+\langle\delta^2(Y_1+Y_2)\rangle<1$ and $\langle\delta^2(X_2-X_3)\rangle+\left\langle\delta^2\left(g_1Y_1+Y_2+Y_3\right)\right\rangle<1$, $\langle\delta^2(X_3-X_1)\rangle+\left\langle\delta^2\left(Y_1+g_2Y_2+Y_3\right)\right\rangle<1$, $\langle\delta^2(X_1-X_2)\rangle+\left\langle\delta^2\left(Y_1+Y_2+g_3Y_3\right)\right\rangle<1$. Where g_1, g_2 and g_3 are the optical gain adjustable factor. Such inseparability criterion can be adjusted by the dressing field and nonlinear gain. If these inequalities are established, the correlation variance is smaller than the corresponding SNL. In this case, the output field is a CV entangled state of the optical field. The smaller the correlation variance is, the higher the entanglement degree is.

2.2. Multi-mode entanglement of PA-FWM in atom-like cavity

Generally, considering that the pump fields $\boldsymbol{E}_1$, $\boldsymbol{E}_2$ and $\boldsymbol{E}_3$ are much stronger than three outputs of cascaded SP-FWM ($\boldsymbol{E}_{S1}$,$\boldsymbol{E}_{S2}$ and $\boldsymbol{E}_{S3}$), they are treated as classical fields and quantum fields (described by operators as $\hat{a}_{S1}$, $\hat{a}_{S2}$ and $\hat{a}_{S3}$), respectively. In Λ-type and Λ-V-type energy level system, under the dipole approximation and the rotating wave approximation, the interaction Hamiltonian describing two-mode entanglement can be expressed as

$$\widehat{H}_{I\text{-}2}=\mathrm{i}\hbar\kappa_1\hat{a}_{S2}^{+}\hat{a}_{S3}^{+}+\mathrm{H.c.}. \tag{1}$$

Similarly, the three-mode entanglement can be described by a parametric interaction:

$$\widehat{H}_{I\text{-}3}=\mathrm{i}\hbar\kappa_1\hat{a}_{S1}^{+}\hat{a}_{S2}^{+}+\mathrm{i}\hbar\kappa_2\hat{a}_{S2}^{+}\hat{a}_{S3}^{+}+\mathrm{H.c.}. \tag{2}$$

The equation (2) is responsible for the entanglement among the three cavity modes. Each SP-FWM process generates $\hat{a}_{S1}^{+}$ and $\hat{a}_{S2}^{+}$ in V-type three-level systems and $\hat{a}_{S3}^{+}$ and $\hat{a}_{S2}^{+}$ in Λ-type three-level systems, simultaneously, which represent the Boson-creation operator acting on the electromagnetic excitation of the Stokes and anti-Stokes channel. Where κ_1 and κ_2 are two third-order nonlinear coefficients proportional to the nonlinear susceptibility of the medium and amplitudes of incident fields, namely: $\kappa_{1/1'}=\left|\chi^{(3)}\boldsymbol{E}_2\boldsymbol{E}_3\right|=\left|N\mu_{\mathrm{F}}^2\rho_{S2/S3}^{(3)}/\hbar\varepsilon_0G_{S2/S3}\right|$ and $\kappa_{2/2'}=\left|\chi^{(3)}\boldsymbol{E}_1\boldsymbol{E}_2\right|=\left|N\mu_{\mathrm{F}}^2\rho_{S1/S2}^{(3)}/\hbar\varepsilon_0G_{S1/S2}\right|$. Here, N is the atomic density, and μ_{F} is the dipole matrix element of the FWM transition. Next, we can only consider nonlinear coefficient κ_1 ($\rho_{23S3}^{(3)}$) in two-mode and consider κ_1 ($\rho_{23S3}^{(3)}$) and κ_2 ($\rho_{20S2}^{(3)}$) in three-mode entanglement, simultaneously. The generated entangled photos in the SP-FWM process are related to the nonlinear coefficient κ_i ($i=1, 2$), which can be modified by the dressing effects induced by $\boldsymbol{E}_2$ and $\boldsymbol{E}_3$.

We adopted the dressing perturbation theory to obtain the density-matrix elements of the SP-FWM fields based on the strong-field coupled equations. Under the weak-field limit, the dressed FWM can be considered as a coherent superposition of a pure FWM process. For a Λ-type system, according to the Liouville pathways [13, 18] the density-matrix elements can be obtained by solving the density-matrix equations via the perturbation chain $\rho_{00}^{(0)}\overset{\omega_2}{\rightarrow}\rho_{20}^{(1)}\overset{-\omega_{S3}}{\longrightarrow}\rho_{30}^{(2)}\overset{\omega_3}{\rightarrow}\rho_{20S2}^{(3)}$ (Stokes signal); the corresponding third-order density-matrix elements for $\boldsymbol{k}_{S2}$ are

$$\rho_{20S2}^{(3)}=\frac{-\mathrm{i}G_2G_{S3}^{*}G_3}{d_{20}\Gamma_{30}d_{20}'}, \tag{3}$$

where $G_i=\mu_{ij}\boldsymbol{E}_{ij}/\hbar$, μ_{ij} is the dipole momentum, Γ_{ij} is the transverse decay rate between levels $|i\rangle\rightarrow|j\rangle$, $d_{20}=\Gamma_{20}+\mathrm{i}\Delta_2$, $d_{20}'=\Gamma_{20}+\mathrm{i}\Delta_3$. Similarly, we can obtain the density-matrix element for $\boldsymbol{k}_{S3}$ via the pathway $\rho_{33}^{(0)}\overset{\omega_3}{\rightarrow}\rho_{23}^{(1)}\overset{\omega_{S2}}{\longrightarrow}\rho_{03}^{(2)}\overset{\omega_2}{\rightarrow}\rho_{23}^{(3)}$ (anti-Stokes signal) as

$$\rho_{23S3}^{(3)}=\frac{-\mathrm{i}G_2G_{S2}^{*}G_3}{d_{23}\Gamma_{03}d_{23}'}, \tag{4a}$$

where $d_{23}=\Gamma_{23}+\mathrm{i}\Delta_3$, $d_{23}'=\Gamma_{23}+\mathrm{i}\Delta_2$. And considering the dressing effect of $\boldsymbol{E}_2$, the density-matrix element is given by

$$\rho_{23S3}^{(3)}=\frac{-\mathrm{i}G_2G_{S2}^{*}G_3}{\left(d_{23}+|G_3|^2/\Gamma_{33}+|G_2|^2/d_{03}\right)\Gamma_{03}d_{23}'}, \tag{4b}$$

where $d_{03}=\Gamma_{03}+\mathrm{i}(\Delta_3-\Delta_2)$. The strong pump $\boldsymbol{E}_2$ through dressing splitting level $|2\rangle$ produces homologous primary dressing states $|G_2\pm\rangle$. The Hamiltonian for primary energy can be written as $\widehat{H}'=-\hbar\begin{bmatrix}0 & G_2\\ G_2^{*} & (-1)^i\Delta_2\end{bmatrix}$; from the equation $\widehat{H}'|G_2\pm\rangle=\lambda_{G_2\pm}|G_2\pm\rangle$, we can obtain eigenvalues $\lambda_{G_2+}=(-\Delta_2+\sqrt{\Delta_2^2+4G_2^2})/2$ and $\lambda_{G_2-}=(-\Delta_2-\sqrt{\Delta_2^2+4G_2^2})/2$, which define the position of level $|G_2+\rangle$ and $|G_2-\rangle$ relative to level $|2\rangle$. Considering the sequential double-dressing effect of $\boldsymbol{E}_2$ and $\boldsymbol{E}_4$, we can obtain the density-matrix element

$$\rho_{23S3}^{(3)}=\frac{-\mathrm{i}G_2G_{S2}^{*}G_3}{(d_{23}+|G_3|^2/\Gamma_{33}+|G_2|^2/d_{03}+|G_4|^2/d_{43})\Gamma_{03}d_{23}'}, \tag{4c}$$

where $d_{43}=\Gamma_{43}+\mathrm{i}(\Delta_3-\Delta_4)$. For the sequential double-dressing FWM, the outer dressing field $\boldsymbol{E}_4$ (ω_4, $\boldsymbol{k}_4$, G_4) drives the transition $|4\rangle(\delta_2)\leftrightarrow|2\rangle\gamma_0$, and the inner dressing field $\boldsymbol{E}_2$ dresses level $|2\rangle$ (figure 1(d1)). When $\boldsymbol{E}_2$ and $\boldsymbol{E}_4$ sequentially dress each other, the primarily dressed states $|G_2\pm\rangle$ are split into secondary dressed states $|G_4\pm G_2\pm\rangle$, namely $\boldsymbol{E}_4$ splits $|G_2\pm\rangle$ into $|G_4\pm G_2+\rangle$ if $\Delta_4>0$, or splits $|G_2-\rangle$ into

$|G_4 \pm G_2 -\rangle$ if $\Delta_4 < 0$. The Hamiltonian for secondary energy can be written as $H'' = -\hbar\begin{bmatrix}\Delta_4' & G_4\\ G_4^* & 0\end{bmatrix}$, where $\Delta_4' = \Delta_4 - \lambda_{G_2\pm}$. From the relation $\widehat{H}''|G_4 \pm G_2 \pm\rangle = \lambda_{G_4\pm G_2\pm}|G_4 \pm G_2 \pm\rangle$, we can obtain eigenvalues $\lambda_{G_4\pm G_2+} = (\Delta_4' \pm \sqrt{\Delta_4'^2 + 4|G_4|^2})/2$ or $\lambda_{G_4\pm G_2-} = (\Delta_4' \pm \sqrt{\Delta_4'^2 + 4|G_4|^2})/2$. Because of the double-dressing effect, $\rho_{23S3}^{(3)}$ is modified directly by the intensity G_2^2 and G_4^2.

When considering the parallel double-dressing effect of $\boldsymbol{E}_2$ and $\boldsymbol{E}_4$, the density-matrix element can be given by

$$\rho_{23S3}^{(3)} = \frac{-iG_2G_{S2}^*G_3}{\left(d_{23} + |G_3|^2/\Gamma_{33} + |G_2|^2/d_{03}\right)\Gamma_{03}\left(d_{23}' + |G_4|^2/d_{43}'\right)}. \tag{4d}$$

Where $d_{43}' = \Gamma_{43} + i(\Delta_2 - \Delta_4)$. Here, this double-dressing scheme is called a parallel dressing scheme because the two dressing fields are independent and parallel-dressed levels $|2\rangle$ and $|0\rangle$ (figure 1(d1)), respectively. And two dressing terms $|G_2|^2/[\Gamma_{03} + i(\Delta_3 - \Delta_2)]$ and $|G_4|^2/[\Gamma_{43} + i(\Delta_2 - \Delta_4)]$ are parallel in equation (4*d*).

Last, considering the triple-dressing effect of $\boldsymbol{E}_2$, $\boldsymbol{E}_3$ and $\boldsymbol{E}_4$ simultaneously in figure 1(d2), the density-matrix element is obtained:

$$\rho_{23S3}^{(3)} = \frac{-iG_2G_{S2}^*G_3}{\left(d_{23} + |G_3|^2/\Gamma_{33} + |G_2|^2/d_{03} + |G_4|^2/d_{43}\right)\Gamma_{03}\left(d_{23}' + |G_3|^2/d_{03}'\right)}. \tag{4e}$$

Where $d_{03}' = \Gamma_{03} + i(\Delta_2 - \Delta_3)$. When coupled with single atom-like cavities, the dressing terms G_2^2, G_3^2 and G_4^2 in the denominator (dressing effect) of equation (4), which results from the resonantly induced spontaneous florescence by $\boldsymbol{E}_2$ (equation (4*b*)) or $\boldsymbol{E}_2 + \boldsymbol{E}_4$ (equations (4*c*) and (4*d*)) or $\boldsymbol{E}_2 + \boldsymbol{E}_3 + \boldsymbol{E}_4$ (equation (4*e*)) can cause the vacuum-induced Rabi splitting.

Similarly, in the V-type system we can obtain the density-matrix element for $\boldsymbol{k}_{S1}$ and $\boldsymbol{k}_{S2}$ via the pathway $\rho_{00}^{(0)} \xrightarrow{\omega_2} \rho_{20}^{(1)} \xrightarrow{-\omega_{S2}} \rho_{00}^{(2)} \xrightarrow{\omega_1} \rho_{10}^{(3)}$ (anti-Stokes signal) and $\rho_{00}^{(0)} \xrightarrow{\omega_1} \rho_{10}^{(1)} \xrightarrow{-\omega_{S1}} \rho_{00}^{(2)} \xrightarrow{\omega_1} \rho_{20}^{(3)}$ (Stokes signal) as

$$\rho_{10S1}^{(3)} = \frac{-iG_1G_{S2}^*G_2}{d_{20}d_{00}'d_{10}'}, \tag{5}$$

$$\rho_{20S2}^{(3)} = \frac{-iG_1G_{S1}^*G_2}{d_{10}d_{00}d_{20}''}. \tag{6}$$

Where $d_{10}' = \Gamma_{10} + i\Delta_2$, $d_{00}' = \Gamma_{00} + i(\Delta_2 - \Delta_1)$, $d_{10} = \Gamma_{10} + i\Delta_1$. $d_{00} = \Gamma_{00} + i(\Delta_1 - \Delta_2)$ and $d_{20}'' = \Gamma_{20} + i\Delta_1$.

Last, we calculate amplitude quadrature and phase quadrature summation of three-mode squeezing from the frequency domain. According to the Heisenberg motion equation: $d\hat{a}_i/dt = [\hat{a}_i, H_I]/i\hbar$ and the input-output theory developed by Gardiner and Collett, the motion equations of two-mode can be written as

$$\frac{d\hat{a}_{S2}}{dt} = -i\Delta\hat{a}_{S2} - (\gamma + \gamma_c)\hat{a}_{S2} + \kappa_1\hat{a}_{S3}^+e^{i\theta_p} + \sqrt{2\gamma}\,\hat{a}^{in}{}_{S2}, \tag{7a}$$

$$\frac{d\hat{a}_{S3}}{dt} = -i\Delta\hat{a}_{S3} - (\gamma + \gamma_c)\hat{a}_{S3} + \kappa_1\hat{a}_{S2}^+e^{i\theta_p} + \sqrt{2\gamma}\,\hat{a}_{S3}^{in}. \tag{7b}$$

Additionally, the motion equations of three-mode can be obtained as

$$\frac{d\hat{a}_{S1}}{dt} = -i\Delta\hat{a}_{S1} - (\gamma + \gamma_c)\hat{a}_{S1} + \kappa_1\hat{a}_{S2}^+e^{i\theta_p} + \sqrt{2\gamma}\,\hat{a}^{in}{}_{S1}, \tag{8a}$$

$$\frac{d\hat{a}_{S2}}{dt} = -i\Delta\hat{a}_{S2} - (\gamma + \gamma_c)\hat{a}_{S2} + \kappa_1\hat{a}_{S1}^+e^{i\theta_p} + \kappa_2\hat{a}_{S3}^+e^{i\theta_p} + \sqrt{2\gamma}\,\hat{a}_{S2}^{in}, \tag{8b}$$

$$\frac{d\hat{a}_{S3}}{dt} = -i\Delta\hat{a}_{S3} - (\gamma + \gamma_c)\hat{a}_{S3} + \kappa_2\hat{a}_{S2}^+e^{i\theta_p} + \sqrt{2\gamma}\,\hat{a}_{S2}^{in}. \tag{8c}$$

Where $\hat{a}_i^{in}$ ($i = S1, S2$ and $S3$) denotes the injected field operator, θ_p is the relative phase between pump lights and the seeding lights, γ denotes the decay rate of signals, and γ_c is the inter-cavity losses.

Taking the Fourier transformation $\widehat{O}(\omega) = \int dt\widehat{O}(t)e^{-i\omega t}/\sqrt{2\pi}$ of equations (7) and (8), we can get $\hat{a}_{S2}$ and $\hat{a}_{S3}$ of two-mode and $\hat{a}_{S1}$, $\hat{a}_{S2}$ and $\hat{a}_{S3}$ of three-mode. The amplitude and phase operator are described with the electromagnetic field annihilation operator $\hat{a}_i = \widehat{X}_i + i\widehat{Y}_i$ and the commutation relation is $[\hat{a}_i, \hat{a}_i^+] = 1$. Then, considering boundary condition $a_i^o(\omega) = \sqrt{2\gamma}\,a_i(\omega) - a_i^{in}(\omega)$ the inseparability criterion of the two-mode entanglement state is given by

$$\begin{aligned}&\left\langle\delta^2(\widehat{X}_{S2}^0 - \widehat{X}_{S3}^0)\right\rangle + \left\langle\delta^2(\widehat{Y}_{S2}^0 + \widehat{Y}_{S3}^0)\right\rangle\\ &= \left\{\left[(\gamma \mp \kappa_1)^2 - \gamma_c^2 - (\Delta + \omega)^2\right]^2 \times \left(\left\langle\delta^2\widehat{X}_{d_2}^{in}(\omega)\right\rangle + \left\langle\delta^2\widehat{Y}_{d_1}^{in}(\omega)\right\rangle\right)\right.\\ &\quad \left. + 4\gamma^2(\Delta + \omega)^2 \times \left(\left\langle\delta^2\widehat{X}_{d_1}^{in}(\omega)\right\rangle + \left\langle\delta^2\widehat{Y}_{d_2}^{in}(\omega)\right\rangle\right)\right\} /\\ &\quad \left[(\gamma + \gamma_c)^2 + (\Delta + \omega)^2 - \kappa_1^2\right]^2 < 1.\end{aligned} \tag{9}$$

Where $\widehat{X}_{d_1}^{in} = (\widehat{X}_{S2}^{in} + \widehat{X}_{S3}^{in})/\sqrt{2}$, $\widehat{X}_{d_2}^{in} = (\widehat{X}_{S2}^{in} - \widehat{X}_{S3}^{in})/\sqrt{2}$, $\widehat{Y}_{d_1}^{in} = (\widehat{Y}_{S2}^{in} + \widehat{Y}_{S3}^{in})/\sqrt{2}$, $\widehat{Y}_{d_2}^{in} = (\widehat{Y}_{S2}^{in} - \widehat{Y}_{S3}^{in})/\sqrt{2}$. $\widehat{X}_{d_1}^{in}$, $\widehat{X}_{d_2}^{in}$, $\widehat{Y}_{d_1}^{in}$ and $\widehat{Y}_{d_2}^{in}$ are the amplitude quadrature summation, and difference, phase quadrature summation and difference, respectively. Equation (9) intimates that two-mode entanglement is determined by nonlinear coefficient κ_1.

Similarly, the inseparability criterion of three-mode entanglement with $\theta_p = 0$ is given by

$$\left\langle \delta^2(\widehat{X}^0_{S2}-\widehat{X}^0_{S3})\right\rangle+\left\langle \delta^2(g_1\widehat{Y}^0_{S1}+\widehat{Y}^0_{S2}+\widehat{Y}^0_{S3})\right\rangle=\frac{1}{(\eta^2-\kappa^2)^2\eta^4}\Bigg\{\Bigg\{\Big[g_1 2\gamma(\eta^2-\kappa_2^2)+2\gamma\kappa_1\kappa_2\Big]^2(\Delta+\omega)^2$$
$$+\ 4\gamma^2\kappa_1^2\Big[\eta^2-\kappa_2(\gamma+\gamma_c)\Big]^2\Bigg\}\left\langle \delta^2\widehat{X}^{\rm in}_{S1}(\omega)\right\rangle+\Bigg\{[2\gamma\kappa_2\eta^2-2\gamma(\eta^2-\kappa_1^2)+(\eta^2-\kappa^2)\eta^2]^2$$
$$+\Big[g_1 2\gamma\kappa_1\kappa_2+2\gamma(\eta^2-\kappa_1^2)\Big]^2(\Delta+\omega)^2\Bigg\}\left\langle \delta^2\widehat{X}^{\rm in}_{S3}(\omega)\right\rangle$$
$$+\Bigg\{\Big[g_1 2\gamma(\eta^2-\kappa_2^2)(\gamma+\gamma_c)-2\gamma\kappa_1\eta^2+2\gamma\kappa_1\kappa_2(\gamma+\gamma_c)-(\eta^2-\kappa^2)\eta^2\Big]^2+4\gamma^2\kappa_1^2\kappa_2^2(\Delta+\omega)^2\Bigg\}\left\langle \delta^2\widehat{Y}^{\rm in}_{S1}(\omega)\right\rangle$$
$$+\Bigg\{\Big[g_1 2\gamma\kappa_1\kappa_2(\gamma+\gamma_c)-2\gamma\kappa_2\eta^2+2\gamma(\eta^2-\kappa_1^2)(\gamma+\gamma_c)-(\eta^2-\kappa^2)\eta^2\Big]^2+4\gamma^2(\eta^2-\kappa_1^2)^2(\Delta+\omega)^2\Bigg\}\left\langle \delta^2\widehat{Y}^{\rm in}_{S3}(\omega)\right\rangle\Bigg\}$$
$$+\frac{1}{(\eta^2-\kappa^2)^2}\Bigg\{\Bigg\{\Big[2\gamma(\gamma+\gamma_c)-2\gamma\kappa_2-\eta^2+\kappa^2\Big]^2+4\gamma^2(\Delta+\omega)^2\Bigg\}\left\langle \delta^2\widehat{X}^{\rm in}_{S2}(\omega)\right\rangle$$
$$+\Bigg\{\Big\{2\gamma[-g_1\kappa_1-\kappa_2+(\gamma+\gamma_c)]-\eta^2+\kappa^2\Big\}^2+4\gamma^2(\Delta+\omega)^2\Bigg\}\left\langle \delta^2\widehat{Y}^{\rm in}_{S2}(\omega)\right\rangle\Bigg\}<1, \tag{10a}$$

$$\left\langle \delta^2(\widehat{X}^0_{S3}-\widehat{X}^0_{S1})\right\rangle+\left\langle \delta^2(\widehat{Y}^0_{S1}+g_2\widehat{Y}^0_{S2}+\widehat{Y}^0_{S3})\right\rangle=\frac{1}{(\eta^2-\kappa^2)^2\eta^4}\Bigg\{\Bigg\{\Big[2\gamma(\gamma+\gamma_c)(\eta^2-\kappa_2^2-\kappa_1\kappa_2)-(\eta^2-\kappa^2)\eta^2\Big]^2$$
$$+\ 4\gamma^2(\Delta+\omega)^2(\eta^2-\kappa_2^2+\kappa_1\kappa_2)^2\Bigg\}\left\langle \delta^2\widehat{X}^{\rm in}_{S1}(\omega)\right\rangle+\Bigg\{\Big[2\gamma(\gamma+\gamma_c)(\kappa_1\kappa_2-\eta^2+\kappa_1^2)+(\eta^2-\kappa^2)\eta^2\Big]^2$$
$$+\ 4\gamma^2(\Delta+\omega)^2(\kappa_1\kappa_2+\eta^2-\kappa_1^2)^2\Bigg\}\left\langle \delta^2\widehat{X}^{\rm in}_{S3}(\omega)\right\rangle$$
$$+\Bigg\{\Big[2\gamma(\eta^2-\kappa_2^2)(\gamma+\gamma_c)-g_2 2\gamma\kappa_1\eta^2+2\gamma\kappa_1\kappa_2(\gamma+\gamma_c)-(\eta^2-\kappa^2)\eta^2\Big]^2+4\gamma^2(\Delta+\omega)^2(\eta^2-\kappa_2^2-\kappa_1\kappa_2)^2\Bigg\}\left\langle \delta^2\widehat{Y}^{\rm in}_{S1}(\omega)\right\rangle$$
$$+\Bigg\{\Big[2\gamma\kappa_1\kappa_2(\gamma+\gamma_c)-g_2 2\gamma\kappa_2\eta^2+2\gamma(\eta^2-\kappa_1^2)(\gamma+\gamma_c)-(\eta^2-\kappa^2)\eta^2\Big]^2+4\gamma^2(\Delta+\omega)^2(\eta^2-\kappa_1^2-\kappa_1\kappa_2)^2\Bigg\}\left\langle \delta^2\widehat{Y}^{\rm in}_{S3}(\omega)\right\rangle\Bigg\}$$
$$+\frac{1}{(\eta^2-\kappa^2)^2}\Bigg\{[4\gamma^2(\kappa_1-\kappa_2)^2+4\gamma^2g_2^2(\Delta+\omega)^2]\left\langle \delta^2\widehat{X}^{\rm in}_{S2}(\omega)\right\rangle+\Big\{2\gamma[-\kappa_1-\kappa_2+g_2(\gamma+\gamma_c)]-\eta^2+\kappa^2\Big\}^2\left\langle \delta^2\widehat{Y}^{\rm in}_{S2}(\omega)\right\rangle\Bigg\}<1, \tag{10b}$$

$$\left\langle \delta^2(\widehat{X}^0_{S1}-\widehat{X}^0_{S2})\right\rangle+\left\langle \delta^2(\widehat{Y}^0_{S1}+\widehat{Y}^0_{S2}+g_3\widehat{Y}^0_{S3})\right\rangle=\frac{1}{(\eta^2-\kappa^2)^2\eta^4}\Bigg\{\Bigg\{\Big[2\gamma(\eta^2-\kappa_2^2)(\gamma+\gamma_c)-2\gamma\kappa_1\eta^2-(\eta^2-\kappa^2)\eta^2\Big]^2$$
$$+\ 4\gamma^2(\Delta+\omega)^2\Big(\eta^2-\kappa_2^2+g_3\kappa_1\kappa_2\Big)^2\Bigg\}\left\langle \delta^2\widehat{X}^{\rm in}_{S1}(\omega)\right\rangle+4\gamma^2\Bigg\{(\Delta+\omega)^2\Big[\kappa_1\kappa_2+g_3(\eta^2-\kappa_1^2)\Big]^2$$
$$+\ 4\gamma^2\kappa_2^2\Big[\kappa_1(\gamma+\gamma_c)-\eta^2\Big]^2\Bigg\}\left\langle \delta^2\widehat{X}^{\rm in}_{S3}(\omega)\right\rangle$$
$$+\Bigg\{\Big[2\gamma(\eta^2-\kappa_2^2)(\gamma+\gamma_c)-2\gamma\kappa_1\eta+g_3 2\gamma\kappa_1\kappa_2(\gamma+\gamma_c)-(\eta^2-\kappa^2)\eta^2\Big]^2+4\gamma^2(\Delta+\omega)^2(\eta^2-\kappa_2^2)^2\Bigg\}\left\langle \delta^2\widehat{Y}^{\rm in}_{S1}(\omega)\right\rangle$$
$$+\Bigg\{\Big[2\gamma\kappa_1\kappa_2(\gamma+\gamma_c)-2\gamma\kappa_2\eta+g_3 2\gamma(\eta^2-\kappa_1^2)(\gamma+\gamma_c)-(\eta^2-\kappa^2)\eta^2\Big]^2+4\gamma^2(\Delta+\omega)^2\kappa_1^2\kappa_2^2\Bigg\}\left\langle \delta^2\widehat{Y}^{\rm in}_{S3}(\omega)\right\rangle$$
$$+\frac{1}{(\eta^2-\kappa^2)^2}\Bigg\{\Bigg\{4\gamma^2(\Delta+\omega)^2+\Big[2\gamma\kappa_1-2\gamma(\gamma+\gamma_c)+(\eta^2-\kappa^2)\Big]^2\Bigg\}\left\langle \delta^2\widehat{X}^{\rm in}_{S2}(\omega)\right\rangle$$
$$+\Bigg\{\Big\{2\gamma[-\kappa_1-g_3\kappa_2+(\gamma+\gamma_c)]-\eta^2+\kappa^2\Big\}^2+4\gamma^2(\Delta+\omega)^2\Bigg\}\left\langle \delta^2\widehat{Y}^{\rm in}_{S2}(\omega)\right\rangle\Bigg\}<1. \tag{10c}$$

Where $\kappa^2 = \kappa_1^2 + \kappa_2^2$ and $\eta^2 = (\gamma + \gamma_c)^2 + (\Delta + \omega)^2$.$\widehat{X}_i^{\text{in}}$ and $\widehat{Y}_i^{\text{in}}$ are the amplitude and phase quadratures of the input modes. Equations (10*a*)–(10*c*) intimate that three-mode entanglement is related to three optical gain adjustable factors g_1, g_2 and g_3 and two nonlinear coefficients κ_1 and κ_2. The following investigation on quantum-correlation variances is based on the criterion shown in equations (9) and (10*a*)–(10*c*)

3. Numerical simulation and analysis

3.1. Double-dressed two-mode entanglement multichannel in atom-like cavity

In this section we will present the results of the numerical calculation. To simplify the presentation, the parameters are normalized to $\gamma + \gamma_c$. We define SNL as shot-noise limit with nonlinear gain coefficients $G_1(\kappa_1) = \cosh^2(\kappa_1) = 0$ and $G_2(\kappa_2) = \cosh^2(\kappa_2) = 0$, and our condition is SNL = 0 dB. This means the entanglement is equivalent to the correlation variances which lie below zero, and it is 'noise' when the variances are greater than or equal to SNL. When the injection field is a coherent field, and its fluctuations are the same as the vacuum fluctuations, then

$$\left\langle \delta^2 \widehat{X}_{S1}^{\text{in}}(\omega) \right\rangle = \left\langle \delta^2 \widehat{X}_{S2}^{\text{in}}(\omega) \right\rangle = \left\langle \delta^2 \widehat{X}_{S3}^{\text{in}}(\omega) \right\rangle = 1/4,$$
$$\left\langle \delta^2 \widehat{Y}_{S1}^{\text{in}}(\omega) \right\rangle = \left\langle \delta^2 \widehat{Y}_{S2}^{\text{in}}(\omega) \right\rangle = \left\langle \delta^2 \widehat{Y}_{S3}^{\text{in}}(\omega) \right\rangle = 1/4.$$

Firstly, we investigate two-mode entanglement under the influence of the sequential double-dressing effect of the strong pumping beams $\boldsymbol{E}_2$ and $\boldsymbol{E}_3$ in the Λ-type three-level system. Figure 2 shows the 3D and contour-line simulation of the correlation variances $\left\langle \delta^2(\widehat{X}_{S2}^0 - \widehat{X}_{S3}^0) \right\rangle + \left\langle \delta^2(\widehat{Y}_{S2}^0 + \widehat{Y}_{S3}^0) \right\rangle < 1$ via equation (9), which gives the panorama of output cavity mode under different conditions. As declared in [17], we have known the entanglement profile can be modified by a single dressing field through vacuum Rabi splitting, vacuum-induced enhancement and suppression of entanglement. As shown in figures 2(a) and (b), scanning Δ_2 and Δ_3 at $\Delta = 0$ in figure 2(a1) and Δ and Δ_2 (Δ_3) at Δ_3 (Δ_2) = 0 in figure 2(a2) without the dressing effect, it always comes out as an inverted single-peak (one-channel) stand for an all-bright-state, with resonant laser frequency and cavity frequency (i.e. $\Delta_2 = \Delta_3 = \Delta = 0$) the maximum entanglement is −30 dB in figures 2(a1) and (a2). Considering the single dressing effect of $\boldsymbol{E}_2$, the typical vacuum Rabi splitting of entanglement appears when set to $G_2 = 30$ MHz and scan Δ and Δ_3 at $\Delta_2 = 0$ in figure 2(b2), the left and right peaks of figure 2(b2) correspond to the $|G_2+\rangle$ and $|G_2-\rangle$ levels created by $\boldsymbol{E}_2$ as show in figure 2(d1), respectively. The maximum entanglement doublet is located asymmetrically due to $\Delta_2 = 0$ and the maximum entanglement is −20 dB. When scan Δ_2 and Δ at $\Delta_3 = 0$ in figure 2(b3), we can see that the quantum variances profile shows a pure suppression of entanglement duo to real energy level $|2\rangle$ turning into a virtual energy level (dark state) as shown in figure 2(d2), and the dressed suppression condition is $\Delta_2 = \Delta_3 = 0$. Specifically, when Δ_2 and Δ are scanned at $\Delta_3 > 0$ in figure 2(b4), the variances change from pure-suppression (dip) (figure 2(b3)) to left-enhancement (peak)-right-suppression (dip). Here, $\omega_{23} > \omega_3$, the coupling field can only resonate with $|G_2-\rangle$ as shown in figure 2(d3); firstly satisfies the dressed enhancement condition $\Delta_3 + \lambda_{G_2-} = 0$, then the dressed suppression condition $\Delta_2 = \Delta_3$, so the correlation variances is the left-bright-right-dark state (figure 2(b4)). Meanwhile, the anti-crossing behavior of entanglement is obtained in figure 2(b1) when scan Δ_3 and Δ_2 at $\Delta = 0$, which clearly exhibits a dip and two thick peaks (two-channel) in figure 2(b1), the suppression condition is at the line $\Delta_2 = \Delta_3$. From figures 2(a) and (b), we can know that the single-channel entanglement without dressing effect may be split into double channel via single dressing effect, which is decided by the dressing term $|G_2|^2/[\Gamma_{03} + \mathrm{i}(\Delta_3 - \Delta_2)]$ in equation (4*b*).

Next, we consider the sequential double-dressing effect of $\boldsymbol{E}_2$ and $\boldsymbol{E}_4$ influence on entanglement profile in figures 2(c1)–(c6). Through adding a dressing field $\boldsymbol{E}_4$ the triple-channel appears in figures 2(c1), (c2), (c5) and (c6). According to equation (4*c*), the reason why a triple-bright-state or dual-dark state (dressed pictures as illustrated in figure 2(d4)) are generated is that the $\boldsymbol{E}_2$ creates homologous primary dressing states $|G_2\pm\rangle$. Then, $\boldsymbol{E}_4$ is tuned close to one of the primarily dressed states $|G_2-\rangle$ (or $|G_2+\rangle$) and through sequential dressing coupling $|G_2-\rangle$ generates the two secondary dressed states $|G_4 \pm G_2-\rangle$, namely there is interaction and competition between the two dressing fields of sequential mode. The double-dressing vacuum Rabi splitting of entanglement (figure 2(c2)) appears when scan Δ and Δ_3 go from negative to positive at $\Delta_2 = \Delta_4 = 0$. It is an inverted two-dip and three-thin-peak (three-channel) profile generated by sequential $\boldsymbol{E}_2 + \boldsymbol{E}_4$ in figure 2(c2). In this case, both $\boldsymbol{E}_2$ and $\boldsymbol{E}_4$ contribute to two bright states and one dark state but, due to two dressing field windows induced by the $\boldsymbol{E}_2$ and $\boldsymbol{E}_4$, overlap and interact with each other, one of the primary splitting doublets is split into the secondary dressed doublet. The three peaks in figure 2(c2), from left to right, correspond to $|G_2+\rangle$, $|G_4 + G_2-\rangle$ and $|G_4 - G_2-\rangle$ as shown in figure 2(d4). One can see the double-dressing anti-crossing behaviors of entanglement express clearly the three-bright-state (three thick peaks) and dual-dark-state when Δ_2 and Δ_3 are scanned in figure 2(c1) (the maximum entanglement is −15 dB), Δ_2 and Δ_4 are scanned in figure 2(c5) and Δ_3 and Δ_4 are scanned in figure 2(c6), respectively. Here, all of the correlation variances are suppressed twice (two dark states) along two different curves among three plump peaks. When Δ_2 and Δ are scanned at $\Delta_3 = \Delta_4 = 0$ in figure 2(c3), there will be twice the two-photon resonance absorption (figure 2(d5)), so correlation variances are one-bright ($|G_4 + G_2-\rangle$) and two-dark states ($|2\rangle$ and $|G_2-\rangle$), and the dressed suppression condition is $\Delta_2 = \Delta_3 = \pm 30$ MHz. Meanwhile, the double dressed enhancement/suppression of entanglement can be observed when scan Δ_2 and Δ go from negative to positive at $\Delta_4 = 0$ and $\Delta_3 = 10$ MHz in figure 2(c4). As shown in figure 2(d6), first it satisfies the dressing resonance enhancement with

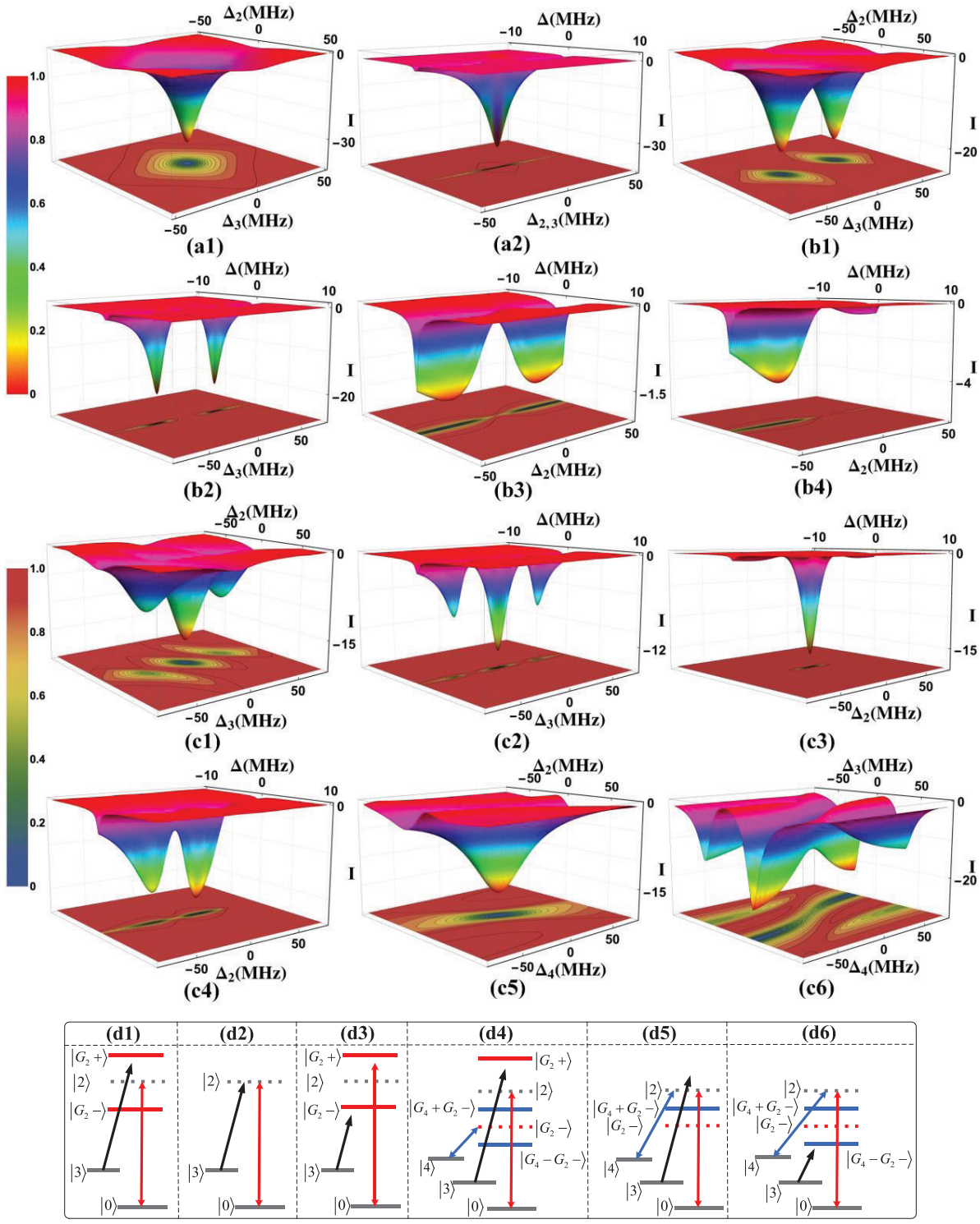

Figure 2. The 3D and contour-line simulation of correlation variances $(I)\left\langle \delta^2(\widehat{X}^0_{S2}-\widehat{X}^0_{S3})\right\rangle+\left\langle \delta^2(\widehat{Y}^0_{S2}+\widehat{Y}^0_{S3})\right\rangle<1$ based on equation (9) with $\widehat{a}^{\rm in}_{S3}$ and $\widehat{a}^{\rm in}_{S2}$ injecting in figure 1(c). Results show that without any dressing fields scan Δ_2 and Δ_3 at $\Delta=0$ in (a1) and scan Δ and Δ_2 (Δ_3) at Δ_3 (Δ_2) $=0$ in (a2); with the single dressing effect of $\boldsymbol{E}_2$ scan Δ_2 and Δ_3 at $\Delta=0$ in (b1), scan Δ and Δ_3 at $\Delta_2=0$ in (b2), scan Δ and Δ_2 at $\Delta_3=0$ in (b3) and scan Δ and Δ_2 at $\Delta_3=10$ MHz in (b4); with the sequential double-dressing effect of $\boldsymbol{E}_2$ and $\boldsymbol{E}_4$ scan Δ_2 and Δ_3 at $\Delta=\Delta_4=0$ in (c1), scan Δ and Δ_3 at $\Delta_2=\Delta_4=0$ in (c2), scan Δ and Δ_2 at $\Delta_3=\Delta_4=0$ in (c3), scan Δ and Δ_2 at $\Delta_3=10$ MHz and $\Delta_4=0$ in (c4), scan Δ_2 and Δ_4 at $\Delta=\Delta_3=0$ in (c5) and scan Δ_3 and Δ_3 at $\Delta=\Delta_2=0$ in (c6), respectively. The zero plane shows the SNL and the two-color bar denotes the normalized intensity value of correlation variances. (d1)–(d6) are the dressed state diagrams.

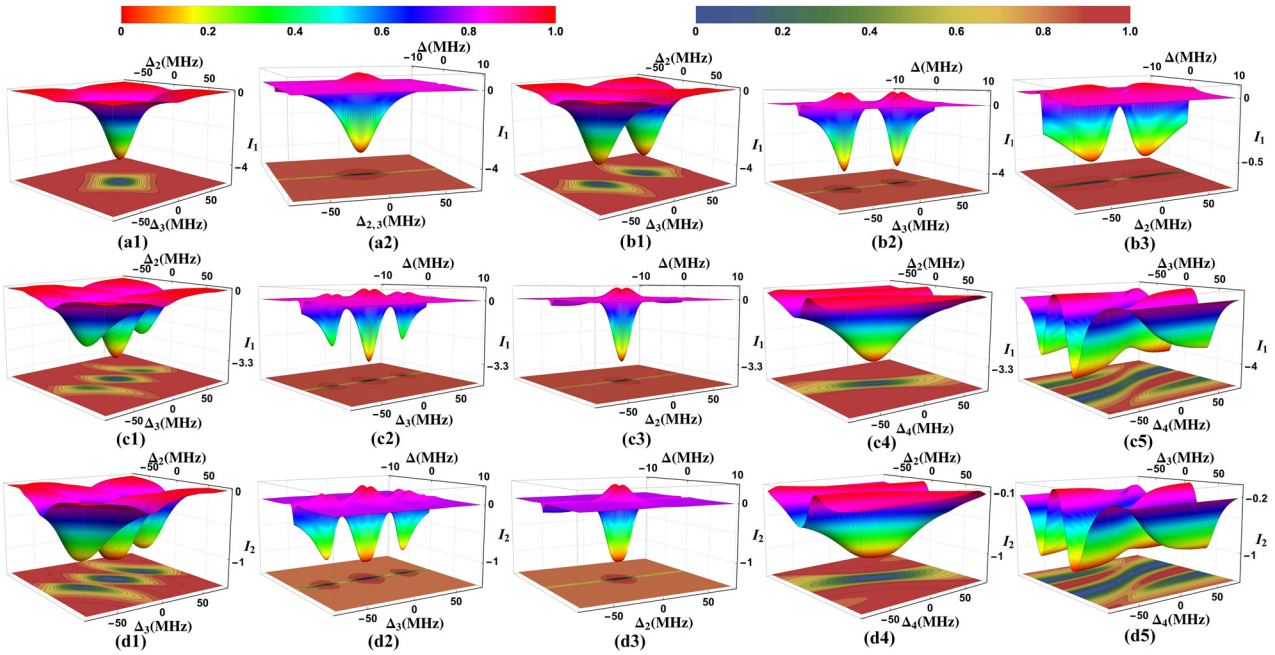

Figure 3. The 3D and contour-line simulation of correlation variances $(I_1)\left\langle\delta^2(\widehat{X}^0_{S2}-\widehat{X}^0_{S3})\right\rangle+\left\langle\delta^2(g_1\widehat{Y}^0_{S1}+\widehat{Y}^0_{S2}+\widehat{Y}^0_{S3})\right\rangle<1$ based on equation (10*a*) with $\widehat{a}^{\rm in}_{S1}$, $\widehat{a}^{\rm in}_{S3}$ and $\widehat{a}^{\rm in}_{S2}$ injecting in figure 1(c). Results show that without dressing effect scan Δ_2 and Δ_3 at $\Delta=0$ in (a1) and scan Δ and Δ_2 (Δ_3) at Δ_3 (Δ_2) $=0$ in (a2); with the single dressing effect of $\boldsymbol{E}_2$ scan Δ_2 and Δ_3 at $\Delta=0$ in (b1), scan Δ and Δ_3 at $\Delta_2=0$ in (b2) and scan Δ and Δ_2 at $\Delta_3=0$ in (b3); with the sequential double-dressing effect of $\boldsymbol{E}_2$ and $\boldsymbol{E}_4$ scan Δ_2 and Δ_3 at $\Delta=\Delta_4=0$ in (c1), scan Δ and Δ_3 at $\Delta_2=\Delta_4=0$ in (c2), scan Δ and Δ_2 at $\Delta_3=\Delta_4=0$ in (c3), scan Δ_2 and Δ_4 at $\Delta=\Delta_3=0$ in (c4) and scan Δ_3 and Δ_4 at $\Delta=\Delta_2=0$ in (c5), respectively. (d1)–(d5) are the same as (c1)–(c5) except with correlation variances (I_2) $\left\langle\delta^2(\widehat{X}^0_{S1}-\widehat{X}^0_{S2})\right\rangle+\left\langle\delta^2(\widehat{Y}^0_{S1}+\widehat{Y}^0_{S2}+g_3\widehat{Y}^0_{S3})\right\rangle<1$ based on equation (10*c*). The zero plane shows the SNL and the two-color bar denotes the normalized intensity value of correlation variances.

$|G_4-G_2-\rangle$, then the dressing absorption suppression with $|G_2-\rangle$, last the dressing enhancement with $|G_4+G_2-\rangle$, so correlation variances are the left-bright-middle-dark-right-bright state (figure 2(c4)). Therefore, the triple-channel entanglement of two-mode can be obtained via sequential double-dressing effect. Similar experimental results for sequential double dressing is obtained in [26], which also verifies the theoretical simulations exhibited in figure 2. Above all, dual-suppression with dual-dark-state denoted by the dressing term $|G_2|^2/[\Gamma_{03}+\mathrm{i}(\Delta_3-\Delta_2)]+|G_4|^2/[\Gamma_{43}+\mathrm{i}(\Delta_3-\Delta_4)]$ in equation (4*c*).

It is worth noting that the diagrams (3D and contour-line) in figures 2(a2), (b2)–(b4) and (c2)–(c4) with scanning cavity detuning and frequency detuning are thinner than those with scanning two-frequency detuning in figures 2(a1), (b1), (c1), (c5) and (c6). It intimates that the cavity has a great influence on entanglement, which induces the lateral squash of entanglement spectrum. In comparison with figures 2(a1), (b1) and (c1), the maximum entanglement significantly reduced with the increase of quantum channels, which complies with the law of conservation of energy.

Overall, two-mode entanglement is determined by dressing enhanced nonlinear gain $G_1(\kappa_1)$. The sequential double dressing can effectively modify the two-mode entanglement process via double vacuum Rabi splitting, dressed anti-crossing behavior and vacuum-induced enhancement/suppression of entanglement, which are induced by the sequential double-dressing term $|G_2|^2/[\Gamma_{03}+\mathrm{i}(\Delta_3-\Delta_2)]+|G_4|^2/[\Gamma_{43}+\mathrm{i}(\Delta_3-\Delta_4)]$. Such quantum three channels may increase the number of possible users or can be applied in secret sharing in a three-user.

3.2. Multi-dressed three-mode entanglement multichannel in atom-like cavity

We know that with nonlinear gain $G_1(\kappa_1)$ increasing the two-mode entanglement degree also increases. However, in such TC-FWM processes, three optical gain adjustable factors g_1, g_2 and g_3 and two nonlinear gains $G_1(\kappa_1)$ and $G_2(\kappa_2)$ have different controllability for different nonseparability criteria. In studying three-mode states, we are often interested in which subsystems are responsible for the entanglement. Here, we simulate quantum correlation variances $\left\langle\delta^2(\widehat{X}^0_{S2}-\widehat{X}^0_{S3})\right\rangle+\left\langle\delta^2(g_1\widehat{Y}^0_{S1}+\widehat{Y}^0_{S2}+\widehat{Y}^0_{S3})\right\rangle<1$, $\left\langle\delta^2(\widehat{X}^0_{S3}-\widehat{X}^0_{S1})\right\rangle+\left\langle\delta^2(\widehat{Y}^0_{S1}+g_2\widehat{Y}^0_{S2}+\widehat{Y}^0_{S3})\right\rangle<1$ and $\left\langle\delta^2(\widehat{X}^0_{S1}-\widehat{X}^0_{S2})\right\rangle+\left\langle\delta^2(\widehat{Y}^0_{S1}+\widehat{Y}^0_{S2}+g_3\widehat{Y}^0_{S3})\right\rangle<1$ under the same condition and considering $g_1=g_2=g_3=1$, so the differences of three modes are determined by three quadrature-amplitude difference correlations $\left\langle\delta^2(\widehat{X}^0_{S2}-\widehat{X}^0_{S3})\right\rangle$, $\left\langle\delta^2(\widehat{X}^0_{S3}-\widehat{X}^0_{S1})\right\rangle$ and

$\left\langle \delta^2(\widehat{X}^0_{S1} - \widehat{X}^0_{S2}) \right\rangle$ (three squeezing states). The satisfaction of any pair of above inequalities is sufficient for full inseparability of three modes. It determines the following discussion about three-mode entanglement between criteria $\left\langle \delta^2(\widehat{X}^0_{S2} - \widehat{X}^0_{S3}) \right\rangle + \left\langle \delta^2(g_1\widehat{Y}^0_{S1} + \widehat{Y}^0_{S2} + \widehat{Y}^0_{S3}) \right\rangle < 1$ and $\left\langle \delta^2(\widehat{X}^0_{S1} - \widehat{X}^0_{S2}) \right\rangle + \left\langle \delta^2(\widehat{Y}^0_{S1} + \widehat{Y}^0_{S2} + g_3\widehat{Y}^0_{S3}) \right\rangle < 1$.

Figure 3 explains the sequential double-dressing effect of $\boldsymbol{E}_2$ and $\boldsymbol{E}_4$ influence on three-mode entanglement. It is seen from figure 3 that the correlation variances $\left\langle \delta^2(\widehat{X}^0_{S2} - \widehat{X}^0_{S3}) \right\rangle + \left\langle \delta^2(g_1\widehat{Y}^0_{S1} + \widehat{Y}^0_{S2} + \widehat{Y}^0_{S3}) \right\rangle < 1$ and $\left\langle \delta^2(\widehat{X}^0_{S1} - \widehat{X}^0_{S2}) \right\rangle + \left\langle \delta^2(\widehat{Y}^0_{S1} + \widehat{Y}^0_{S2} + g_3\widehat{Y}^0_{S3}) \right\rangle < 1$ are smaller than the SNL. This indicates that the CV tripartite entanglement criterion is satisfied. At the same time, the entanglement is accompanied by multispatial mode in each mode. And one can see that the variances profile of three-mode entanglement with sequential double dressing are similar to two-mode, as shown in figure 2; all phenomena illustrated in figure 3 can be explained as before. This means that the profile of three-mode entanglement can be controlled via enhanced nonlinear gain $G_1(\kappa_1)$. Similarly, $\boldsymbol{E}_2$ creates homologous primary dressing states $|G_2+\rangle$ & $|G_2-\rangle$ and splits the single-photon resonant peak (figures 3(a1) and (a2)) into a doublet (figures 3(b1) and (b2)) located at $\Delta_2 = \pm G_2 = \pm 30$ MHz. Then, the outer dressing field $\boldsymbol{E}_4$ can exactly hit on one of the primary dressed state (such as $|G_2-\rangle$), and create the secondarily dressed states $|G_4 \pm G_2-\rangle$. Reflecting on variances spectra, the single inverted dip in figure 3(b3) is split into two inverted dips and a peak, as illustrated in figures 3(c3) and (d3). The remaining pattern profiles of quantum correlation variances are same as figure 2, so here we do not display this again for simplicity. This indicates that three-mode entanglement three-channel can be achieved via sequential double dressing as well. Meantime, comparing the 3D simulations of quantum correlation variances between $\left\langle \delta^2(\widehat{X}^0_{S2} - \widehat{X}^0_{S3}) \right\rangle + \left\langle \delta^2(g_1\widehat{Y}^0_{S1} + \widehat{Y}^0_{S2} + \widehat{Y}^0_{S3}) \right\rangle < 1$ and $\left\langle \delta^2(\widehat{X}^0_{S1} - \widehat{X}^0_{S2}) \right\rangle + \left\langle \delta^2(\widehat{Y}^0_{S1} + \widehat{Y}^0_{S2} + g_3\widehat{Y}^0_{S3}) \right\rangle < 1$ in figures 3(c1)–(c5) and (d1)–(d5), we can find that the graphs have similar entanglement spectra except that the maximum entanglement is different (-3.3 dB in figures 3(c1)–(c5) and -1 dB in figures 3(d1)–(d5)). Namely, the only difference is the degree of squeezing $\left\langle \delta^2(\widehat{X}^0_{S2} - \widehat{X}^0_{S3}) \right\rangle > \left\langle \delta^2(\widehat{X}^0_{S1} - \widehat{X}^0_{S2}) \right\rangle$. As a matter of fact, the TC-FWM processes are based on the effective vacuum-induced SP process in equation (2) and the quantum PA process in equation (8), which generated Stokes photons $\hat{a}^+_{S1}$ and $\hat{a}^+_{S3}$, has similar quantum characteristics. Essentially, three-mode entanglement coming from TC-FWM processes can approximate two two-mode entanglement processes that origin from $G_1(\kappa_1)$ and $G_2(\kappa_2)$, respectively. Then, variances $\left\langle \delta^2(\widehat{X}^0_{S2} - \widehat{X}^0_{S3}) \right\rangle$ and $\left\langle \delta^2(\widehat{X}^0_{S1} - \widehat{X}^0_{S2}) \right\rangle$ are mainly determined by $G_1(\kappa_1)$ (and can be modified by the dressing field in the Λ-type system) and $G_2(\kappa_2)$, respectively. Through dressing controlling $G_1(\kappa_1) > G_2(\kappa_2)$ we acquire $\left\langle \delta^2(\widehat{X}^0_{S2} - \widehat{X}^0_{S3}) \right\rangle > \left\langle \delta^2(\widehat{X}^0_{S1} - \widehat{X}^0_{S2}) \right\rangle$. It is also worth mentioning that the degree of three-mode entanglement is far less than two-mode entanglement when comparing with figures 2 and 3. Here, both gain $G_1(\kappa_1)$ and $G_2(\kappa_2)$ compete with each other and affect three-mode entanglement in a Λ-V-type cascade system, which leads to a reduction in the effective gain. Besides, the SP-SWM is generated from internal cascading the two SP-FWM; the coexistence of TC-FWM and SWM also influences the degree of three-mode entanglement, so the generated three-photon in TC-FWM is still far less than the two-photon procedure in SP-FWM. Last but not least, the nonseparability criteria for three-mode entanglement are stricter (at least simultaneously satisfying two of three criteria) than two-mode (only one criterion).

Taking it all into account, figure 3 demonstrates that three-mode entanglement comes from the coupling of two nonlinear gains $G_1(\kappa_1)$ and $G_2(\kappa_2)$. The enhanced $G_1(\kappa_1)$ plays a dominant role which can control and optimize the profile of three-mode entanglement as well as two-mode. The degree of two-mode entanglement is bigger than three-mode entanglement. Meanwhile, three-channel entanglement of three-mode can also be achieved by a sequential double-dressing effect in atom-like media as well as two-mode. Such three channels can be used in QKD to realize secure key one-to-triple distribution and nonlocal quantum imaging. The quality of imaging (e.g. the contrast and resolution) is significantly improved compared with the two-mode entanglement and can be well controlled by multiple parameters.

Next, we focus on three-mode entanglement dressed by the parallel double-dressing effect of $\boldsymbol{E}_2$ and $\boldsymbol{E}_4$ as shown in figures 4(a1)–(a6). From figure 3 we know different entanglement criteria have the same entanglement structure spectra, so in the following discussion we only concentrate on entanglement criterion $\left\langle \delta^2(\widehat{X}^0_{S2} - \widehat{X}^0_{S3}) \right\rangle + \left\langle \delta^2(g_1\widehat{Y}^0_{S1} + \widehat{Y}^0_{S2} + \widehat{Y}^0_{S3}) \right\rangle < 1$. We can see the profiles of parallel double-dressing correlation variances $\left\langle \delta^2(\widehat{X}^0_{S2} - \widehat{X}^0_{S3}) \right\rangle + \left\langle \delta^2(g_1\widehat{Y}^0_{S1} + \widehat{Y}^0_{S2} + \widehat{Y}^0_{S3}) \right\rangle < 1$ in figures 4(a1)–(a6) have significant differences with the sequential double dressing in figures 2 and 3. In comparison with the sequential double dressing makes three-channel entanglement in figures 2(c1), (c2), (c5), (c6) and 3(c1), (c2), (c5), (d1), (d2), (d5). We may observe four-channel entanglement with the parallel double dressing in figures 4(a1), (a5) and (a6). Here, the four thick peaks (four channels) in the spectra come from $\boldsymbol{E}_2 + \boldsymbol{E}_4$ inducing two kinds of splitting. In the dressed picture, $\boldsymbol{E}_2$ and $\boldsymbol{E}_4$ are parallel and independently drive the transition from $|2\rangle \rightarrow |0\rangle$ and $|4\rangle \rightarrow |2\rangle$, then create four dressed states $|G_2\pm\rangle$ and $|G_4\pm\rangle$, as shown in figure 4(c1). Two dressing-field windows induced by $\boldsymbol{E}_2$ and $\boldsymbol{E}_4$ separate with each other. The double-dressing anti-crossing behavior clearly expresses four bright states (four peaks) $|G_2\pm\rangle$ and $|G_4\pm\rangle$ and two dark states $|2\rangle$ and $|0\rangle$ induced by two dressing fields together when scan Δ_2 and Δ_3 at $\Delta_3 = \Delta_4 = 0$ in figure 4(a1), when scan Δ_2 and

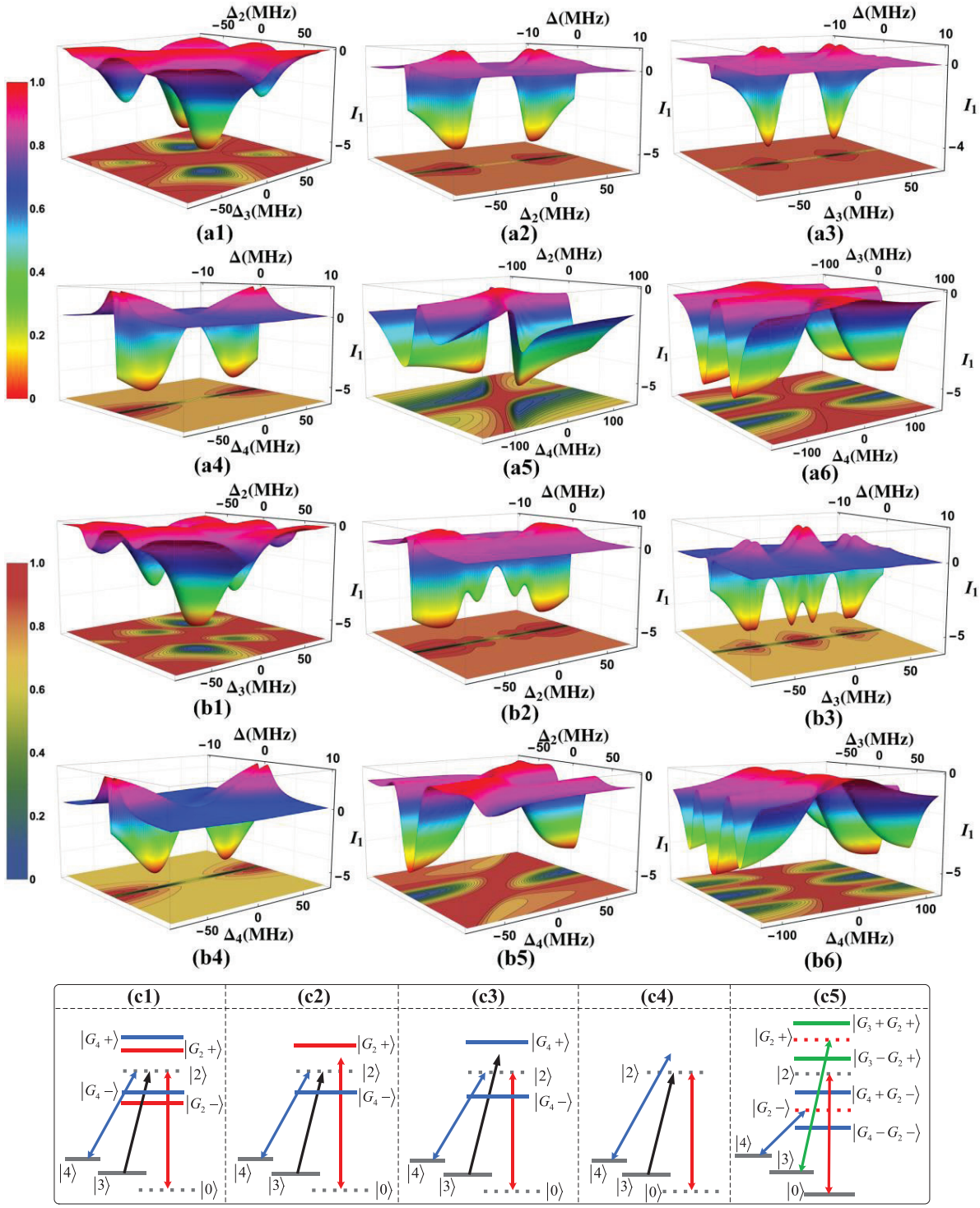

Figure 4. The 3D and contour-line simulation of correlation variances $(I_1)\left\langle \delta^2(\hat{X}^0_{S2}-\hat{X}^0_{S3})\right\rangle+\left\langle \delta^2(g_1\hat{Y}^0_{S1}+\hat{Y}^0_{S2}+\hat{Y}^0_{S3})\right\rangle<1$ based on equation (10*a*) with $\hat{a}^{\rm in}_{S1}$, $\hat{a}^{\rm in}_{S3}$ and $\hat{a}^{\rm in}_{S2}$ injecting in figure 1(c). Results show that with the parallel double-dressing effect of $\boldsymbol{E}_2$ and $\boldsymbol{E}_4$ scan Δ_2 and Δ_3 at $\Delta=\Delta_4=0$ in (a1), scan Δ and Δ_2 at $\Delta_3=\Delta_4=0$ in (a2), scan Δ and Δ_3 at $\Delta_2=\Delta_4=0$ in (a3), scan Δ and Δ_4 at $\Delta_2=\Delta_3=0$ in (a4), scan Δ_2 and Δ_4 at $\Delta=\Delta_3=0$ in (a5) and scan Δ_3 and Δ_4 at $\Delta=\Delta_2=0$ in (a6), respectively. (b1)–(b6) are the same as (a1)–(a6) except with the triple-dressing effect of $\boldsymbol{E}_2$, $\boldsymbol{E}_3$ and $\boldsymbol{E}_4$. The zero plane shows the SNL and the two-color bar denotes the normalized intensity value of correlation variances. (c1)–(c6) are the dressed state diagrams.

Δ_4 at $\Delta=\Delta_3=0$ figure 4(a5) and when scan Δ_3 and Δ_4 at $\Delta=\Delta_2=0$ in figure 4(a6). Simultaneously, these correlation variances also are suppressed twice along the line $\Delta_2=0$ and $\Delta_2=\Delta_3$, as illustrated in figure 4(a1), along the line $\Delta_2=0$ and $\Delta_2=\Delta_4$ in figure 4(a5) and along the line $\Delta_3=0$ and $\Delta_4=0$ in figure 4(a6). Figures 4(a2) and 4(a3) show that there are two pairs of vacuum Rabi splitting induced by G_2 and G_4 (dressed state diagram as shown in

figures 4(c2) and (c3)), respectively. However, there is also a difference in figures 4(a2) and (a3) due to Δ_2 playing different roles in the two dressing terms $|G_2|^2/[\Gamma_{03}+\mathrm{i}(\Delta_3-\Delta_2)]$ and $|G_4|^2/[\Gamma_{43}+\mathrm{i}(\Delta_2-\Delta_4)]$. When scan Δ and Δ_2 at $\Delta_3=\Delta_4=0$ only with $|G_2|^2/[\Gamma_{03}+\mathrm{i}(\Delta_3-\Delta_2)]$, we should obtain a pure suppression of entanglement such as in figures 2(b3) and 3(b3), or else with $|G_4|^2/[\Gamma_{43}+\mathrm{i}(\Delta_2-\Delta_4)]$, the standard vacuum Rabi splitting dual peaks will appear as illustrated in figures 2(b2) and 3(b2). Then, we can see that the profile of entanglement in figure 4(a2) is the two dressing terms $|G_2|^2/[\Gamma_{03}+\mathrm{i}(\Delta_3-\Delta_2)]$ and $|G_4|^2/[\Gamma_{43}+\mathrm{i}(\Delta_2-\Delta_4)]$ interacting as a consequence. When scan Δ and Δ_3 at $\Delta_2=\Delta_4=0$ in figure 4(a3), it displays a vacuum Rabi splitting doublet of entanglement (decided by $|G_2|^2/[\Gamma_{03}+\mathrm{i}(\Delta_3-\Delta_2)]$). Similarly, by scanning Δ and Δ_4, a pure suppression of entanglement (dressed state diagram as shown in figure 4(c4)) comes from $|G_4|^2/[\Gamma_{43}+\mathrm{i}(\Delta_2-\Delta_4)]$ in figure 4(a4). The positions of these enhanced peaks are determined by the homologous Rabi frequency and the dressing field detuning: here, $\Delta_3=\pm G_4=\pm 30$ MHz, $\Delta_2=\pm G_2=\pm 30$ MHz. According to dressed state analysis and equation (4*d*), the suppressed-dip conditions in figures 4(a2) and (a4) are $\Delta_2=\Delta_3=0$ and $\Delta_4=\Delta_3=0$, respectively. Here, parallel double dressing splits up four channels, all of double vacuum Rabi splitting; dressed anti-crossing behavior and vacuum-induced enhancement/suppression are induced by the dressing terms $|G_2|^2/[\Gamma_{03}+\mathrm{i}(\Delta_3-\Delta_2)]$ and $|G_4|^2/[\Gamma_{43}+\mathrm{i}(\Delta_2-\Delta_4)]$.

Figures 4(b1)–(b6) show the triple-dressing effect of $\boldsymbol{E}_2$, $\boldsymbol{E}_3$ and $\boldsymbol{E}_4$ and its influence on three-mode entanglement. In particular, we can see the correlation variances $\left\langle \delta^2(\widehat{X}^0_{S2}-\widehat{X}^0_{S3})\right\rangle+\left\langle \delta^2(g_1\widehat{Y}^0_{S1}+\widehat{Y}^0_{S2}+\widehat{Y}^0_{S3})\right\rangle<1$ exhibiting six thick peaks (six channels) in figures 4(b1) and (b6), i.e. triplet anti-crossing behaviors appear with three dark states (the triple dressed phenomenological model, as shown in figure 4(c5)) when triplet splitting acts on three-mode entanglement. It results from the competition between the multi-dressed effect of $|G_3|^2/[\Gamma_{03}+\mathrm{i}(\Delta_2-\Delta_3)]$ and $|G_2|^2/[\Gamma_{03}+\mathrm{i}(\Delta_3-\Delta_2)]+|G_4|^2/[\Gamma_{43}+\mathrm{i}(\Delta_3-\Delta_4)]$ in equation (4*e*). When scan Δ_2 and Δ_3 at $\Delta=\Delta_4=0$, the correlation variances illustrate the dark states along the line $\Delta_2=0$, $\Delta_3=0$ and $\Delta_2=\Delta_3$ in figure 4(b1). When scan Δ_3 and Δ_4 at $\Delta_2=\Delta_4=0$, figure 4(b6) illustrates orthogonal double ' + ' shape vacuum-induced suppression (three dark states) of entanglement along the line $\Delta_3=\pm 30$ MHz and $\Delta_4=0$. In comparison with figures 4(b5) and 2(c5), we can see that the mid peak in figure 2(c5) is spit into double peaks by the dressing effect of $\boldsymbol{E}_4$ when Δ_2 and Δ_4 are scanned at $\Delta_2=\Delta_4=0$ in figure 4(b5). Specifically, when scan Δ and Δ_2 at $\Delta_3=\Delta_4=0$ (as shown in figure 4(b2)), there are also three dark states from the first dressing effect leading to the suppression of entanglement, as shown in figures 2(b3) and 3(b3); then the second and third dressing split into two dips at $\Delta_2=\pm 30$ MHz, respectively. Similarly, the triple vacuum Rabi splitting of entanglement appears in figure 4(b3) when scan Δ and Δ_3 at $\Delta_2=\Delta_4=0$, which come from the double vacuum Rabi splitting (as shown in figures 2(c2) and 3(c2), (d2)). Moreover, the middle peak (figure 4(b3)) at $\Delta_3=0$ is dressed, splitting two peaks. When scan Δ and Δ_4 at $\Delta_2=\Delta_3=0$ in figure 4(b4), there is a pure suppression dip as shown in figure 4(a4). Further, our numerical results show the lateral squeezing effect of the cavity and that an increase in the cavity detuning Δ leads to a significant decrease the degree of three-mode entanglement in figures 4(a2)–(a4) and (b2)–(b4). It is worth mentioning that the switching between multichannels can be used for QKD that realizes secure key one-to-multiple distribution.

Above all, when considering triple-dressing progression of $\boldsymbol{E}_2$, $\boldsymbol{E}_3$ and $\boldsymbol{E}_4$, the homologous three dressing-field windows induced by the $\boldsymbol{E}_2$, $\boldsymbol{E}_3$ and $\boldsymbol{E}_4$ will interfere each other, and simultaneously the duo to self-dressing effect of $\boldsymbol{E}_2$ and $\boldsymbol{E}_3$, the whole process in figures 4(b1)–(b6) are very complex and difficult to analyze. The triple anti-crossing behaviors, vacuum Rabi splitting and enhancement/suppression of entanglement are derived from triple dressing. All of them are the consequence of interaction between dressing terms $|G_3|^2/[\Gamma_{03}+\mathrm{i}(\Delta_2-\Delta_3)]$ and $|G_2|^2/[\Gamma_{03}+\mathrm{i}(\Delta_3-\Delta_2)]+|G_4|^2/[\Gamma_{43}+\mathrm{i}(\Delta_3-\Delta_4)]$. As discussed above, figures 3 and 4 show the any-cavity mode of three-mode entanglement can be effectively modified by the multi-dressed effect through switching the dressed multichannel. We may use the multichannel of three-mode entanglement to share arbitrary quantum states among multi-users at once and realize nonlocal quantum imaging without a beam splitter.

4. Conclusion

In summary, we use FWM and TC-FWM in Pr^{3+}: YSO vapor to generate two- and three-mode entanglement states of the electromagnetic field. Additionally, the influence of the multi-dressing PA-FWM process on two- and three-mode entanglement has been discussed theoretically. We can conclude that the degree of three-mode entanglement is determined by the coupling of two nonlinear gains. The three-mode entanglement profile can be controlled and optimized by the multi-dressing field via multiple vacuum Rabi splitting, enhancement/suppression and anti-crossing behaviors of entanglement as well as two-mode. Specifically, both two- and three-mode entanglement with single and sequential double dressing can give rise to two and three quantum channels, as shown in figures 2 and 3, and three-mode entanglement with parallel double and triple dressing leads to four and six quantum channels in figure 4, respectively. The triple-mode entanglement state proposed in the current work can be used for the implementation of a triple-mode entangled source, where the generation efficiency of the entangled triple-beam and degree of entanglement will be significantly enhanced by nonlinear susceptibility and quantum gain. This shows that entanglement channels can be distributed to many parties for QKD, effectively increasing the number of available channels from one channel.

Acknowledgments

This work was supported by the 973 program (No.2012CB921804), the National Nature Science Foundation of China (No. 61308015, 11474228, 61605155), and the Key Scientific and Technological Innovation Team of Shaanxi Province (No. 2014KCT-10).

References

[1] Zhou L, Yang L, Li Y and Sun C P 2013 Quantum routing of single photons with a cyclic three-level system *Phys. Rev. Lett.* **111** 103604
[2] Fang J, Huang P and Zeng G 2014 Multichannel parallel continuous variable quantum key distribution with Gaussian modulation *Phys. Rev.* A **89** 2
[3] Patel K A, Dynes J F, Lucamarini M, Choi I, Sharpe A W, Yuan Z L, Penty R V and Shields A J 2014 Quantum key distribution for 10 Gb s^{-1} dense wavelength division multiplexing networks *Appl. Phys. Lett.* **104** 051123
[4] Duan L M, Lukin M D, Cirac J I and Zoller P 2001 Long-distance quantum communication with atomic ensembles and linear optics *Nature* **414** 413–8
[5] Giovannetti V, Lloyd S and Maccone L 2004 Quantum-enhanced measurements: beating the standard quantum limit *Science* **306** 1330–6
[6] Brida G, Genovese M and Ruo Berchera I 2010 Experimental realization of sub-shot-noise quantum imaging *Nat. Photon.* **4** 227–30
[7] Burnham D C and Weinberg D L 1970 Observation of simultaneity in parametric production of optical photon pairs *Phys. Rev. Lett.* **25** 84–7
[8] Strekalov D V, Sergienko A V, Klyshko D N and Shih Y H 1995 Observation of two-photon 'ghost' interference and diffraction *Phys. Rev. Lett.* **74** 3600
[9] Zhou Y, Jia X, Li F, Xie C and Peng K 2015 Experimental generation of 8.4 dB entangled state with an optical cavity involving a wedged type-II nonlinear crystal *Opt. Express* **23** 4952–9
[10] Kwiat P G, Mattle K, Weinfurter H, Zeilinger A, Sergienko A V and Shih Y 1995 New high-intensity source of polarization-entangled photon pairs *Phys. Rev. Lett.* **75** 4337–41
[11] Boyer V, Marino A M, Pooser R C and Lett P D 2008 Entangled images from four-wave mixing *Science* **321** 544–7
[12] Fleischhauer M, Imamoglu A and Marangos J P 2005 Electromagnetically induced transparency: optics in coherent media *Rev. Mod. Phys.* **77** 633–73
[13] Zhang Y, Brown A W and Xiao M 2007 Opening four-wave mixing and six-wave mixing channels via dual electromagnetically induced transparency windows *Phys. Rev. Lett.* **99** 123603
[14] Zhang Y, Khadka U, Anderson B and Xiao M 2009 Temporal and spatial interference between four-wave mixing and six-wave mixing channels *Phys. Rev. Lett.* **102** 013601
[15] Yan M, Rickey E G and Zhu Y 2001 Observation of doubly dressed states in cold atoms *Phys. Rev.* A **64** 013412
[16] Qin Z, Cao L, Wang H, Marino A M, Zhang W and Jing J 2014 Experimental generation of multiple quantum correlated beams from hot rubidium vapor *Phys. Rev. Lett.* **113** 023602
[17] Li Z, Wang X, Li C, Zhang Y, Wen F, Ahmed I and Zhang Y 2016 Two-mode entanglement of dressed parametric amplification four-wave mixing in an atomic ensemble *Laser Phys. Lett.* **13** 025402
[18] Li P, Zheng H, Zhang Y, Sun J, Li C, Huang G, Zhang Z, Li Y and Zhang Y 2013 Controlling the transition of bright and dark states via scanning dressing field *Opt. Mater.* **35** 1062–70
[19] Shi W, Hu X and Wang F 2009 Three-mode entanglement and amplification in correlated spontaneous emission lasers *J. Phys. B: At. Mol. Opt. Phys.* **42** 165506
[20] Gupta P, Horrom T, Anderson B E, Glasser R and Lett P D 2016 Multichannel entanglement distribution using spatial multiplexing from four-wave mixing in atomic vapor *J. Mod. Opt.* **63** 185–9
[21] Lim H C, Yoshizawa A, Tsuchida H and Kikuchi K 2008 Broadband source of telecom-band polarization-entangled photon-pairs for wavelength-multiplexed entanglement distribution *Opt. Express* **16** 16052–7
[22] Herbauts I, Blauensteiner B, Poppe A, Jennewein T and Hübel H 2013 Demonstration of active routing of entanglement in a multi-user network *Opt. Express* **21** 29013–24
[23] van Loock P and Furusawa A 2003 Detecting genuine multipartite continuous-variable entanglement *Phys. Rev.* A **67** 052315
[24] Li C, Wang L, Zheng H, Lan H, Lei C, Zhang D, Xiao M and Zhang Y 2014 All-optically controlled fourth- and sixth-order fluorescence processes of Pr^{3+}: YSO *Appl. Phys. Lett.* **104** 051912
[25] Bai Y and Han S 2007 Ghost imaging with thermal light by third-order correlation *Phys. Rev.* A **76** 043828
[26] Li N, Zhao Z, Chen H, Li P, Li Y, Zhao Y, Zhou G, Jia S and Zhang Y 2012 Observation of dressed odd-order multi-wave mixing in five-level atomic medium *Opt. Express* **20** 1912–29